Sensors and Actuators A 314 (2020) 112029

Contents lists available at ScienceDirect

Sensors and Actuators A: Physical

journal homepage: www.elsevier.com/locate/sna

# Highly elastic capacitive pressure sensor based on smart textiles for full-range human motion monitoring

Chi Cuong Vu, Jooyong Kim *

*Department of Organic Materials and Fiber Engineering, Soongsil University, Seoul 156-743, People's Republic of China*

ARTICLE INFO

*Article history:*
Received 29 December 2019
Received in revised form 13 March 2020
Accepted 24 April 2020
Available online 7 May 2020

*Keywords:*
Spacer fabric
Capacitive pressure sensor
Adaptive fuzzy-neuro network
Gait analysis

ABSTRACT

Human motion analysis has become an important clinical step for collecting data in the healthcare field. However, the typical movement monitorings have to be faced with many different challenges about tools, reliability, and working range of sensors for applications at different positions on the human body. To fulfill this aim, the design and fabrication of a multi-purpose capacitive pressure textile sensor for wearable electronics applications are presented. Because of the high elasticity of the dielectric layer of spacer fabric, the capacitive pressure sensor exhibits a very fast recovery time (7 ms) and high cycling stability (> 20,000). Besides, the stacking structure of the electrode layers (SWCNT/Silver paste) due to excellent durability even under large deformations (grasping, bending, stretching), and breathable for the skin in applications. As the practical demonstrations, the pressure sensors are embedded into a textile glove for grasp motion monitoring, and smart socks for walking gait analysis during activities of daily living. More importantly, an adaptive fuzzy-neuro network algorithm has been developed and adapted in order to increase the accuracy of the gait monitoring system under actual and realistic wearing test conditions.



## 1. Introduction

Wearable sensors, especially the textile sensors or fabric sensors, have become mainstream these days and attracted great interest from researchers. Through their special structures, the textile sensors present physical flexibility and typical size that cannot be achieved with other existing electronic manufacturing techniques. Many studies on the development of fabric sensors and their physical characteristics have been conducted in the last years [1–4]. These studies include flexible pressure [5,6], strain [7], temperature [8,9], and electromagnetic sensors [10]. Amongst these sensors, the pressure sensors have become one of the most vigorously studied research fields. The pressure textile sensors enable close-fitting on curvilinear surfaces or direct attachment to clothes that are highly important in the new generation of portable and wearable electronics [11,12]. There are many studies in order to design and fabricate pressure sensors in soft robotics [13], human physiological monitoring, health care [14–16], human-machine interface [17], power sources [13,18], flexible electronic components [19,20], etc.

Most of the operating mechanisms of pressure sensors are based on a relationship between pressure and electrical properties such as resistance [21], piezoelectric voltages [22], and capacitance [23] of constituent conductive materials. To date, the capacitive soft sensors have dominated research in this field due to excellent performance and better stability than resistive soft sensors. Besides, many studies were effectively proven to be capacitive pressure textile sensors highly suitable for wearable devices [24–26]. However, one of the critical disadvantages characteristics for those capacitive pressure sensors is to necessitate the use of complex fabrication methods, high-cost, or a lack of suitable signal processing algorithms. These characteristics limit the possibility of mass production or application in a realistic product.

This research developed a proper combination of the textile sensor fabrication based on single-walled carbon nanotubes (SWCNT) [27], stretchable silver ink [28–30], encapsulation paste [31], and thin spacer fabric [32]. The silver paste layers help the sensors to have conductivity, flexibility, and stretchability in wearable device applications. Besides, the SWCNT layers will ensure rapid recovery of the conductivity under working cycles. Furthermore, the encapsulation/PET yarn layer will guarantee the constant and robust elastic of sensor structure even under large deformations. The characteristic of the fabricated sensor would be analyzed in the paper. We also showed an application of this sensor on the glove for monitoring finger motion. Especially, to accelerate the convergence of smart textiles and machine learning algorithms, we developed an adaptive neuro-fuzzy network (ANFIS) [33–37] in order to monitor

* Corresponding author.
*E-mail address:* jykim@ssu.ac.kr (J. Kim).

https://doi.org/10.1016/j.sna.2020.112029
0924-4247/

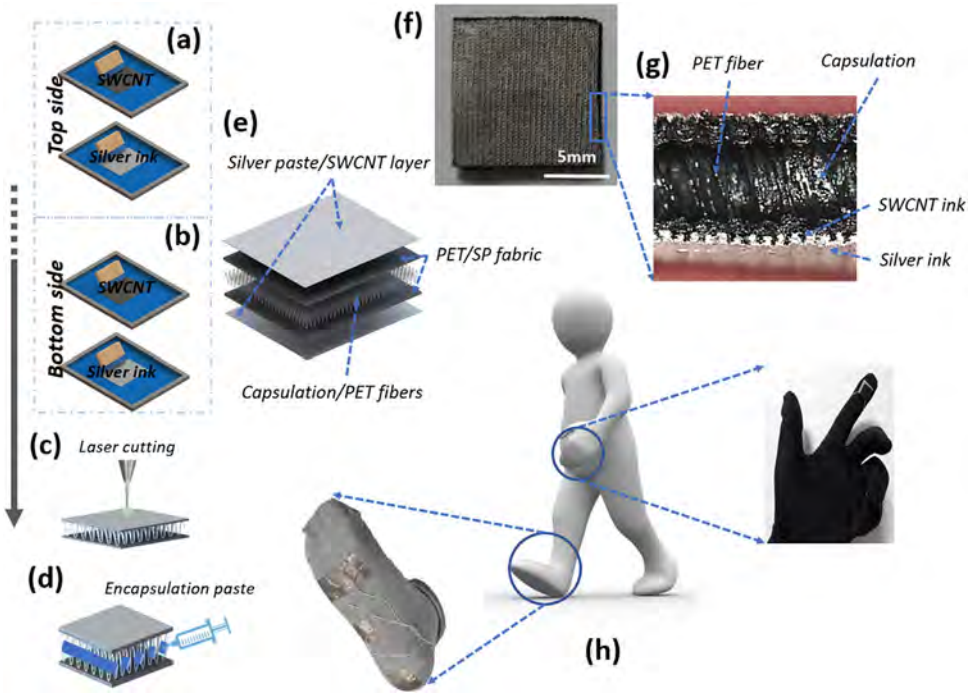


**Fig. 1.** The manufacturing process of capacitive pressure sensor consisting of (a) Printing SWCNT/Silver paste on the top side of the spacer fabric, (b) Printing SWCNT/Silver paste on the bottom side of the spacer fabric, (c) Shaping the sensors by the laser cutting, (d) Injecting capsulation paste into the spacer layer, (e) Structure of the fabricated sensor, (f) Real image of the sensor, (g) Cross-section of the sensor, and (h) Two applications of the sensors.

human gait [38,39] by analyzing data from the smart socks integrated the sensors. Data of human gait obtained through the smart socks would be processed and analyzed on a computer-based on the adaptive neuro-fuzzy network model in order to perform the best gait phase classification.

## 2. Materials and methods

### 2.1. Materials

The polyester/spandex (PET/SP) fabrics are made by co-weaving spandex with polyester with a ratio of 76/24 from SNT Co. Ltd., Seoul, Korea. The conventional multifilament yarns of PET/SP fabrics with high elasticity and recovery. These fibers can be converted into conductive fibers via soaking, padding, or surface treatment. Besides, the PET/SP spacer fabrics have 3D manufactured textile structures in which two outer textile layers (PET/SP fabric layers) are connected by a layer of pile fibers (PET yarns). This structure has the properties of crush resistance, high compression resilience, and a 3D appearance. In the research, we used SWCNT ink and stretchable silver paste in order to produce the electrode patterns on fabrics. The SWCNT inks were prepared by acid solution from SWCNT powder from KH Chemicals Co. Ltd., Incheon, South Korea. The stretchable silver inks (DM-SIP-2001) and the encapsulation pastes (DM-SIP-2500) were obtained from Dycotec Materials Ltd., United Kingdom.

### 2.2. Fabrication process of the capacitive pressure sensor

The SWCNT inks (0.1 wt %) were stirred and ultra-sonicated in an automatic stirring machine at the temperature of 60–80 °C, time of 2 h, and motor speed of 1000 rpm. The silver pastes were stored in a fridge (4 °C) with lids tightly sealed. This process allows removing air bubbles inside the conductive inks and pastes.

As shown in Fig. 1a, we printed the SWCNTs onto the top side of the spacer fabric by screen printing technologies at the speed of 30 mm/s and dried (180–200 °C) in 10 min. by a two-way drying machine in order to remove the excess water. After that, we printed the Ag pastes and dried again (120–150 °C) in 15 min. in order to remove the solvents. The same processes are applied to the bottom side of the spacer fabric (Fig. 1b). Then, the sensors are shaped by a laser cutting machine in order to create arbitrary, customizable individual shapes (Fig. 1c).

Finally, the encapsulation pastes are injected into the spacer layer (PET yarn layer) and dried (120 °C) in 12 min. (Fig. 1d). At the end of this step, we obtained the capacitive pressure sensors with two electrode layers of highly stretchable Ag/SWCNT layers and separated by an encapsulation/PET yarns layer as the dielectric (Fig. 1e–g). Because of using thin spacer fabric, the final thickness of the sensor is small and fits many wearable applications (Fig. 1h).

## 3. Results and discussion

### 3.1. Structure, working principle

In order to evaluate the electrical response of the proposed sensors, we developed an experimental setup to analyze data using a customized UTM machine (South Korea) (Fig. 2a). Fig. 2b shows the working principle of the capacitive pressure sensor based on parallel-plate capacitances [40,41], and Fig. 2c shows the real working image of the sensor. When the spacer fabric is under pressure, the spacer layer (PET yarns) is bent from the stretching state. When the pressure is released, the spacer layer returns to the initial state. The capacitance is accordingly varying as a function of changes in the distance between parallel-plate electrodes. In wearable applications, the design of the capacitive pressure sensors is complicated by a low elastic of the materials. Otherwise, the outputs are easily influenced by parasitic capacitance. The spacer layer, by PET yarns of the spacer fabric, will improve the elasticity of the electrodes, thereby increasing the sensitivity of the sensor in for the flexible applications.

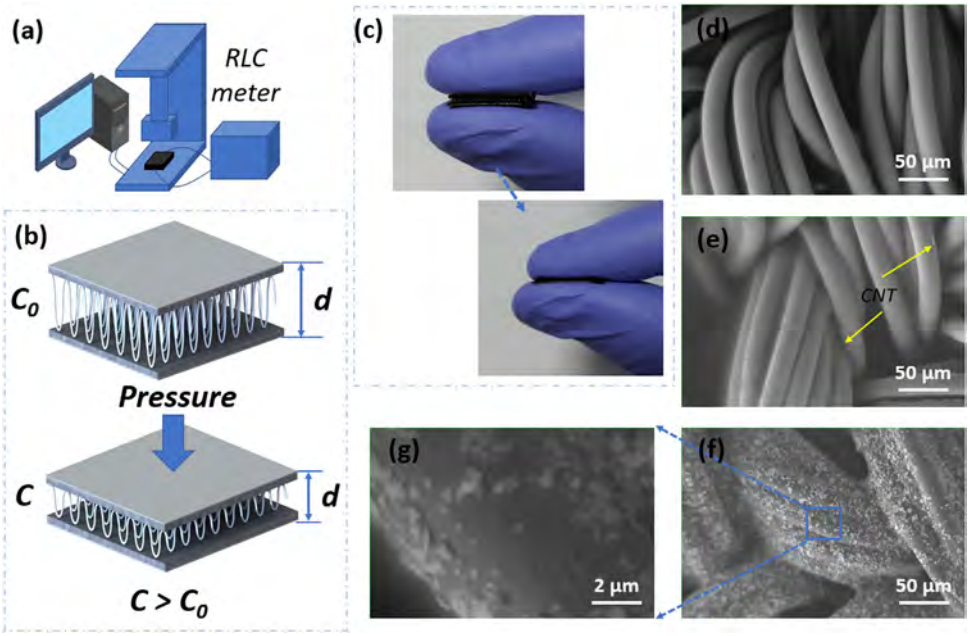


**Fig. 2.** (a) Schematic of the universal testing machine (UTM), (b) Working mechanism of the sensor before and after loading pressure, (c) Real picture of the sensor under loading pressure, (d) Magnified view of the spacer fabric's surface at 50 µm, (e) Magnified view of the sensor's surface at 50 µm after printing SWCNT, (f) Magnified view of the sensor's surface at 50 µm after printing silver paste, (g) Magnified view of the sensor's surface at 2 µm after printing silver paste.

For the spacer fabric-based capacitive pressure sensor, the sensitivity can be calculated as $S = \Delta C/C_0/P$ where P represents the applied pressure, and $\Delta C$ and $C_0$ represent the change in capacitance and baseline capacitance, respectively. The capacitance at the pressing point (C) can be calculated by Eq. 1, where A represents electrode area, d represents dielectric thickness, $\varepsilon_0$ represents constant for dielectric permittivity of vacuum, and $\varepsilon_r$ represents permittivity of dielectric. Following that, the capacitance change relies on the change in dielectric thickness of the spacer fabric.

$$C_{sensor} = \varepsilon_o \varepsilon_r \frac{A}{d_0} \quad (1)$$

The variations of the permittivity of dielectric layers also contribute to a change in capacitance as shown in Eq. 2, where $\varepsilon_{air} = 1$ and $\varepsilon_{PET} = 3.3$. The sensitivity increases when the volume of the air gaps decreases. The decrease in dielectric thickness (d) and the increase in permittivity ($\varepsilon_e$) under pressure together contribute to increasing the sensitivity of the textile capacitance sensor.

$$\varepsilon_e = (\%V_{air}.\varepsilon_{air} + \%V_{PET}.\varepsilon_{PET}) \quad (2)$$

Fig. 2d–g shows SEM images of the standard spacer fabric with the magnified view showing the initial yarns, and the printed yarns with SWCNTs/silver at different steps of the process proposed. The diameter of the single PET yarn is about 10 µm and appears loosely twisted with ample of free space between the microfibers. SWCNT particles could be observed in the form of thin printings and stuck onto PET/SP yarns with a 50 % printing area. Otherwise, the silver conductive layer printed onto CNTs-PET/SP yarns with a 95 % printing area.

### 3.2. Characteristics

Fig. 3a shows the method in order to insert the encapsulation paste [31] into the spacer layer. It is injected by a needle at the speed of 0.5 mm/s, and the diameter of the one encapsulation line is about 0.65 mm. In this research, we evaluated three kinds of structures as 0/3/5 encapsulation lines (S0/S1/S2), respectively. As seen in Fig. 3b, while the samples constructed with 5 encapsulation lines have a pressure sensitivity of $4.2 \times 10^{-2}$ $kPa^{-1}$, the samples with 0 encapsulation lines were $2.05 \times 10^{-2}$ $kPa^{-1}$, and the samples with 3 encapsulation lines were $3.5 \times 10^{-2}$ $kPa^{-1}$, respectively. It is clear that the sensitivity of sensors will increase following the increase of the encapsulation volume at the spacer layer. Otherwise, Fig. 3c and d shows a large working range of the sensors under high pressure (up to 1000 kPa). At the 1000 kPa pressure level, the output signals of the samples were still below the saturation point. However, the sensitivity values of the sensors reduced at this level. From the relative change in the capacitance under pressure levels of different samples, we suggest the sensor with three encapsulation lines in the spacer layer for wearable applications. This structure ensures the sensitivity and the working range of the sensors, as well as the breathable ability for the skin.

Response/recovery time are important parameters for evaluating the performance of the sensor in the dynamic application. The viscoelastic nature of the PET yarns of the spacer fabric is the main reason for a delay time. Fig. 4a shows a fast response/recovery time of 7 ms at 100 kPa. Because of the fast self-recovery process of the PET connections, our sensors demonstrate the rapid recovery of the electrical property and ensure the performance of the device during high pressure or a lot of working cycles. This advantage is mainly caused by the excellent elastic properties of PET/SP spacer fabric, especially the release-ability of PET connections between two parallel-plate electrodes of the capacitive pressure sensor points. We can see that the recovery time would be increased several milliseconds when increasing the capsulation paste in the spacer layer, as shown in Fig. 4b and c. It was caused by the viscoelastic increase with the volume of the capsulation paste. In real applications, a sensor with fast recovery time and a large working range is desirable.

The dynamic durability of the sensors can be evaluated through the stable electrical functionality and mechanical integrity during its loading/unloading cycles. This is mainly caused by the fatigue and plastic deformation of the PET connections under high-pressure, which causes damage to the spacer layers and the sensing nanomaterials (silver bread/SWCNT). The durability performed under lab customized UTM, and the capacitance was measured at every 50 cycles. Attributed to the high elastic recovery performance

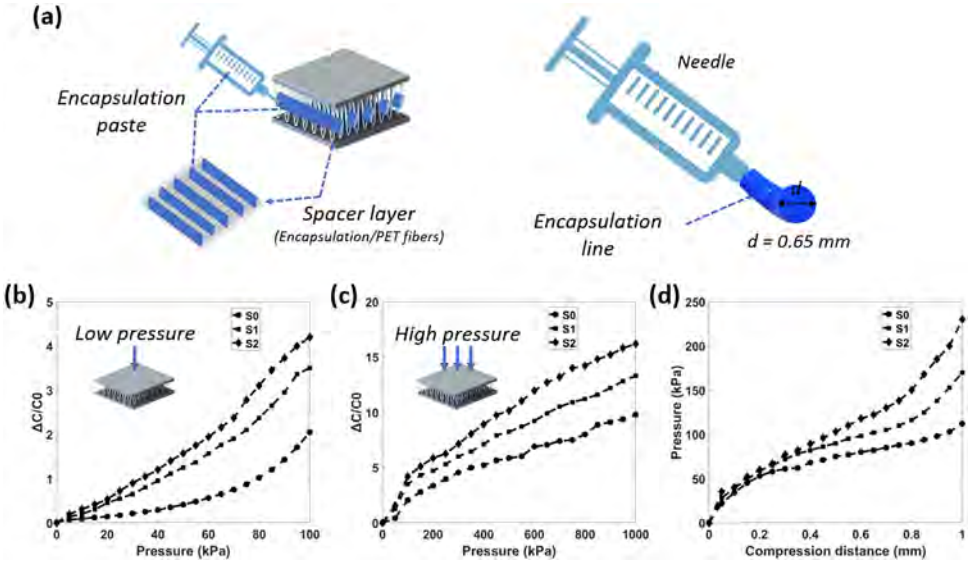


**Fig. 3.** (a) Injecting encapsulation paste into the spacer layer, (b) Relationship between the variation of capacitance and the applied pressure from 0 - 100 kPa, (c) Relationship between the variation of capacitance and the applied pressure from 0 - 1000 kPa, (d) Relationship between the compress distance and the applied pressure.

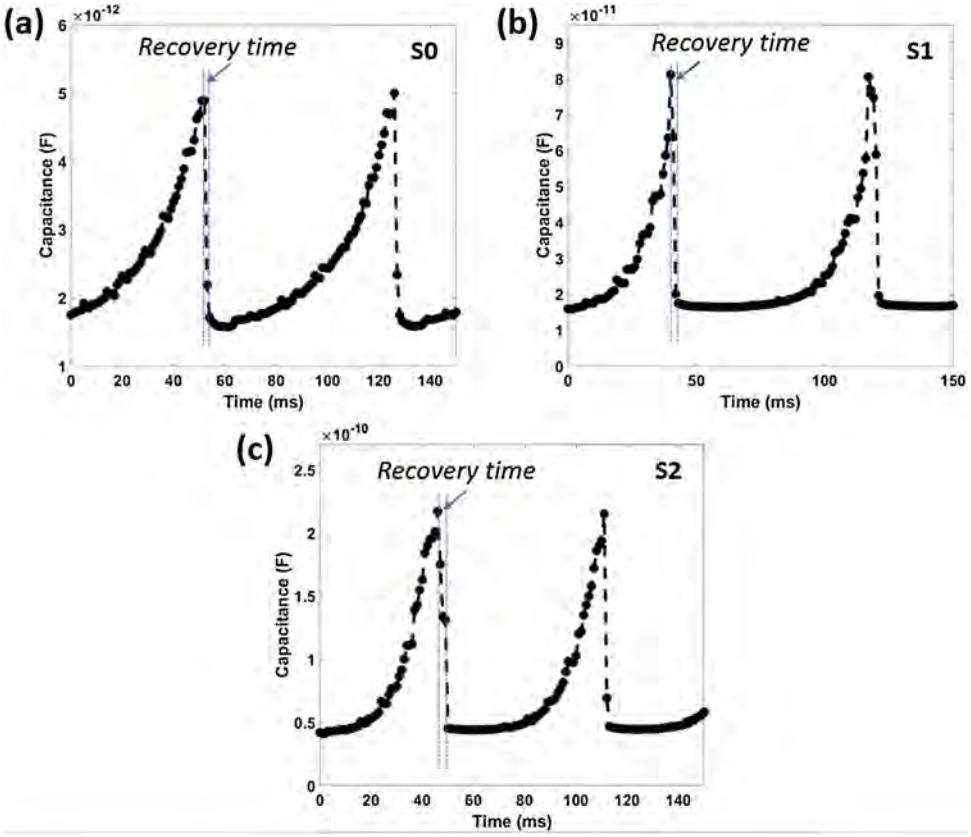


**Fig. 4.** Response/recovery time under pressure 0–100 kPa of (a) The structure with 0 encapsulation line, (b) The structure with three encapsulation lines, and (c) The structure with five encapsulation lines.

of the spacer fabric dielectric layer, the sensors show an intact sensitivity, and a highly reproducible. It was recorded that the uniform capacitive changes of less than 7 % after 20,000 loading/unloading cycles at 100 kPa (Fig. 5a), as well as less than 10 % after 10,000 intensive cycles at 1000 kPa (Fig. 5b). It is worth mentioning that the electric fabric sensor also has high durability to other deformation types. Moreover, we observed that the conductivity of two electrode layers is less than 0.7 Ω when stretching under 30 % (Fig. 5c), bending, and twisting (Fig. 5d), which is significant for wearable applications (Fig. 5e).

Fig. 6a shows the effect of humidity on the performance of the sensors. The capacitance has a little change (< 8 %) in the humidity range of 40 % to 70 %. This is likely due to the relative permittivity of the air inside the spacer layer changes with the humidity. In order to decrease the effect of this factor, we suggest decreasing the volume of the air in the spacer layer by a composite of encapsulation and

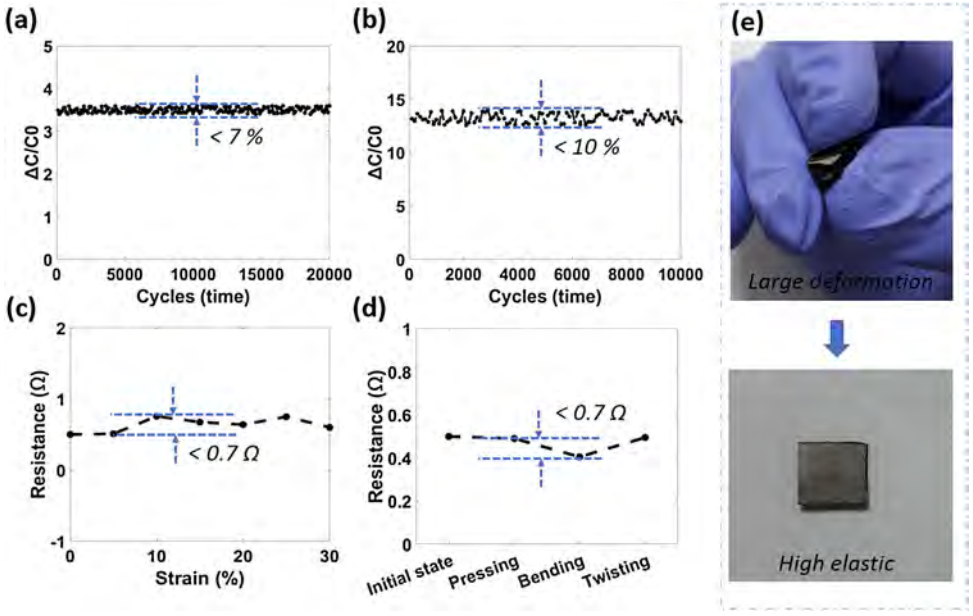


**Fig. 5.** Characteristics of the capacitive pressure sensor consisting of (a) Dynamic durability of the sensor after 20,000 loading/unloading cycles at pressure 100 kPa, (b) Dynamic durability of the sensor after 10,000 loading/unloading cycles at pressure 1000 kPa, (c) Resistance change of the sensor under strain 30 %, (d) Resistance change of the sensor under different deformations, and (e) State of the sensor after large deformation.

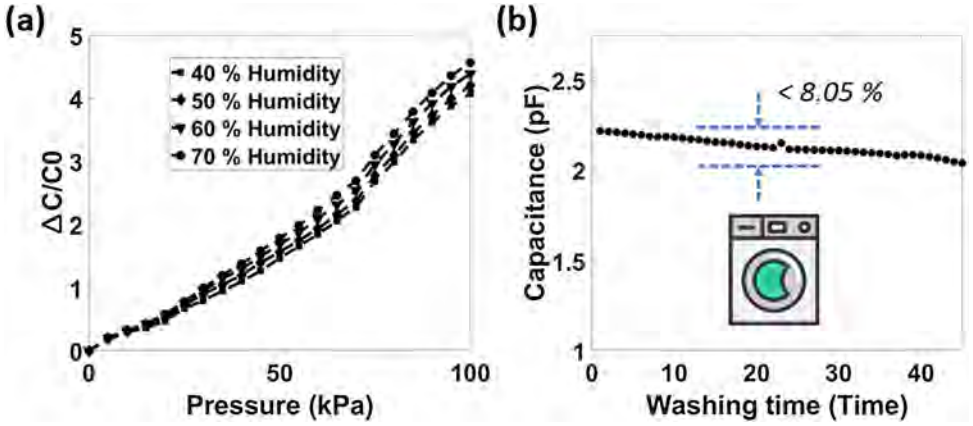


**Fig. 6.** (a) Relationship between the variation of capacitance and humidity, (b) Relationship between the variation of capacitance and washing times.

silicone/sugar [45]. However, this method also will change the sensitivity of the sensors, so it needs more experiments. The e-textile electronics have a major limitation that is the electrode materials (CNTs/silvers) will fall-out after washing. As shown in Fig. 6b, we evaluated the capacitance of the sensors at 100 kPa after a number of washing times. It is clear that the sensors can still work well after 45 washing times. This advantage is mainly caused by the adhesive-ability of silver pastes in order to protect the electrode materials.

We evaluated the sensor performance at different curved surfaces. As described in Fig. 7a and b, curvature stands are 3D printed with varying degrees of 0°, 20°, 30°, 45°, respectively. The sensor is flexed along the 3D-stands. There are slight differences in the capacitance responses between the curved surfaces. Fig. 7c shows a good performance of the sensor at different curved levels from 0° to 30°. However, the capacitance responses will become unstable at 45°. The performance will decrease following the increase of the curved surface. However, the sensor is still stable in small curvature for wearable applications.

Fig. 8 shows an overview comparison of this sensor. Our sensors are thinner than other studies [24,42–44]. The sensors also have better breathable properties than the reference samples in three studies [24,43,44]. Especially, the spacer layers by the PET yarns will have more highly elastic than the silicone [24]. Besides, our sensors showed an excellent working ability at the positions where the large deformations are common. However, the structure still exists a limitation with extremely slight pressures. This is due to decreased sensitivity when increasing the number of PET fibers in the spacer layer. We suggest removing a part of these fibers to ensure the sensitivity of the sensors.

## 4. Smart glove

In order to demonstrate the potential in the wearable application, the proposed sensor was integrated into a smart tactile glove, as shown in Fig. 9a and b. The sensor was shaped at $10 \times 10$ mm dimensions and embedded into the index finger of the glove in order to detect a grasping task. We used an instant adhesive to fix the position of the electronic line and a thermal film to ensure the connection between the electronic line and the electrode of sensors [45]. The subjects were instructed to grasp a plastic cup for an amount of time, and the electrical signal was con-

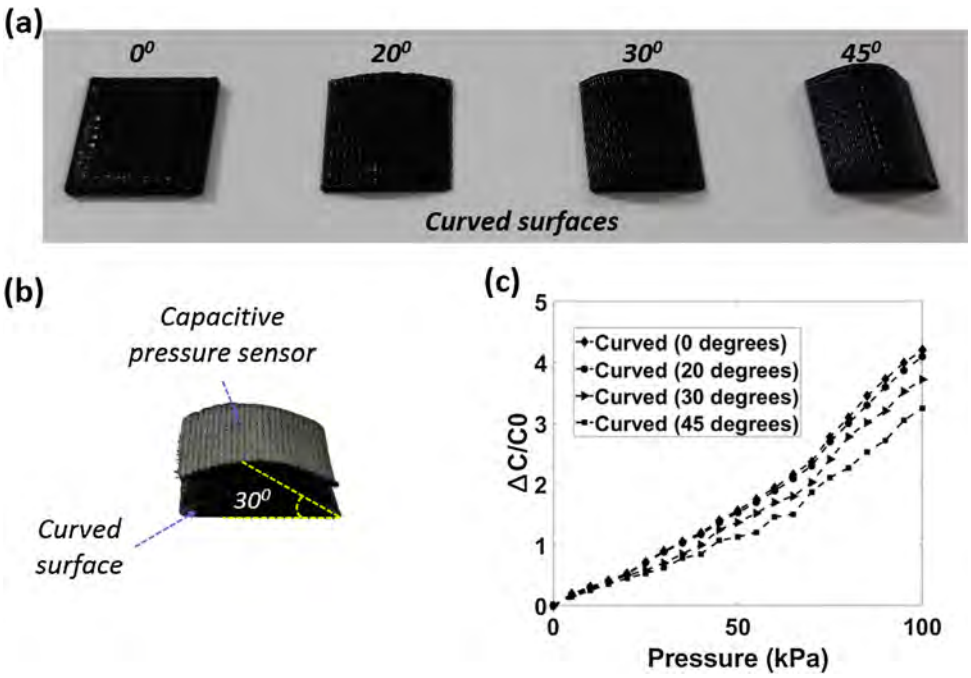


**Fig. 7.** Effect of the curved surfaces, consisting of (a) 3D-printed curved surfaces of 0°, 20°, 30°, and 45°, (b) Experimental setup for performance testing on curvature surfaces, (c) Relationship between the variation of capacitance and curved surface.

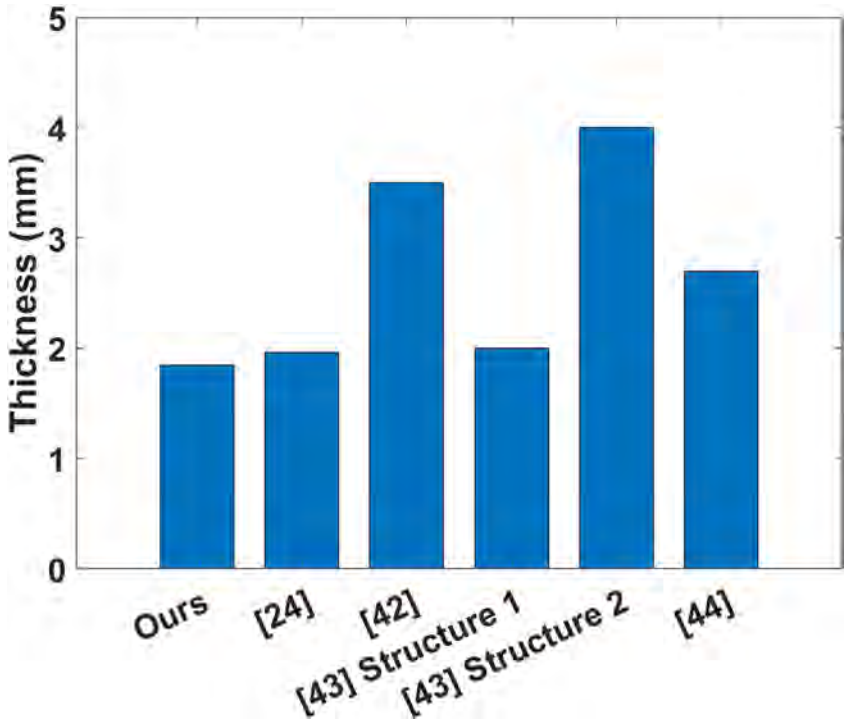


**Fig. 8.** The thickness of the fabricated sensors in comparison with other studies.

tinuously recorded. Hardware flatform of this experimental is an integrated circuit, composed of some main components such as an Arduino Uno (5 V–16 Mhz), Bluetooth module, and lipo-battery (3.7 V) (Fig. 9c). The weight of the cup is 300 g. Fig. 9d shows the capacitance change during the experiment. The capacitance increased when grasping the cup and decreased when releasing the cup. From the result, it is clear that this pressure sensor can be used in soft wearable sensors and actuator applications that require sensitivity.

## 5. Smart socks and human gait analysis

Because of the high elastic and large detection range of the sensor, it can be embedded into the positions on clothes where the

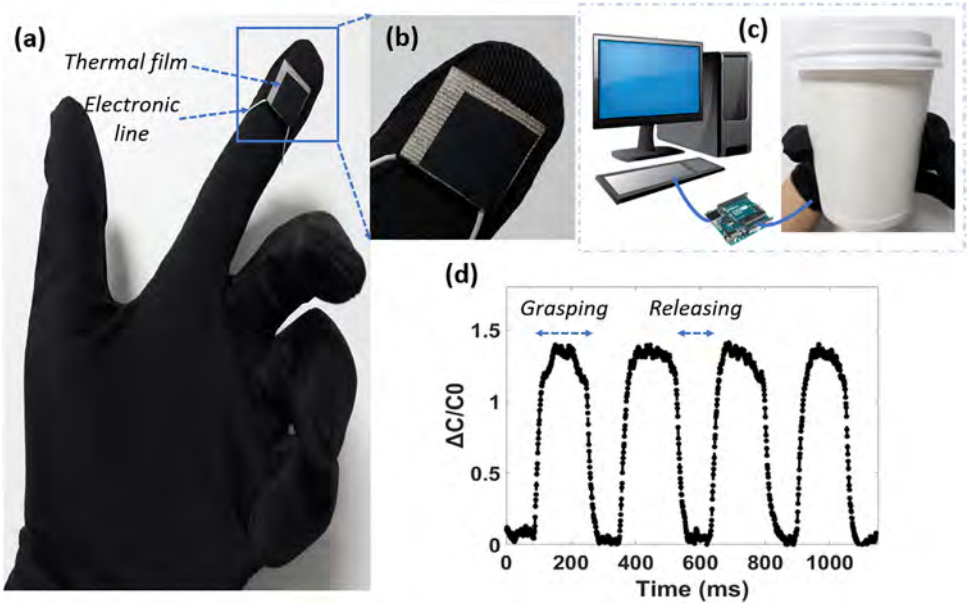


**Fig. 9.** (a) Smart textile glove, (b) Sensor on the index finger of the glove was covered by the thermal film, (c) Diagram of the grasping experimental, and (d) Capacitance change when grasping/releasing the cup.

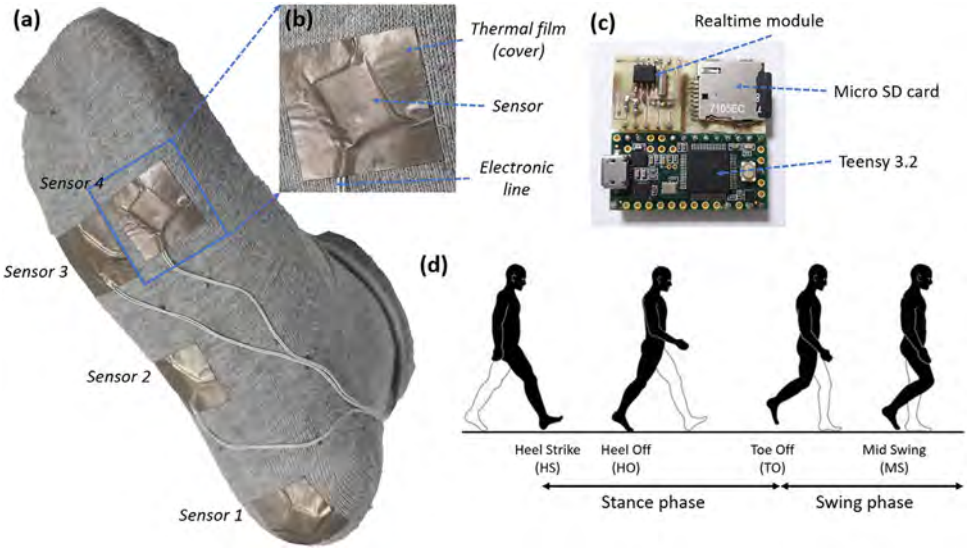


**Fig. 10.** (a) Smart sock, (b) One sensor on the smart sock was covered by the thermal film, (c) Electronic device, and (d) Phases of walking gait.

large deformations are common. In this paper, we proposed the smart socks integrated the pressure sensors in order to distinguish different gaits, as shown in Fig. 10a–c. Subjects have worn the socks and walked on a straight corridor. During the experiment, the capacitance ratio ($\Delta C/C_0$) of each sensor was recorded by utilizing the commercially available Teensy 3.2 module [46]. Fig. 10d shows the phases of walking gait, included heel strike (HS), hell off (HO), toe off (TO), and mid swing (MS). Capacitance change is found to be the highest in the HS of stance phase, and lowest in MS of the swing phase. From the data acquisition of four sensors, we integrated an adaptive neuro-fuzzy network system to classify the phases of walking gait.

ANFIS is one type of artificial neural network that is based on the Takagi and Sugeno FIS. It is a set of fuzzy IF - THEN rules that have learning capability to approximate nonlinear functions. Fig. 11 shows a new architecture of the proposed ANFIS model, which consisted of five layers [47].

The first layer is the fuzzification layer with four input variables (sensor 1 - sensor 4). The condition parameters are utilized to get the degree of elements in a given set as a particular input. Every node in this layer is an adaptive node with a node function:

$$\mu(k; a, b, c) = \frac{1}{1 + \left|\frac{z-a}{b}\right|^{2c}} \tag{3}$$

where k represents several membership functions (MFs), a is the center, b is the function's width, and c is both the direction of the bell and its width.

The second layer is the uniform rule layer. All nodes are the circle nodes, which minimize (AND) or maximize (OR) incoming data, and send the product out.

R= {min[AND]} or {max[OR]}

$$W_i = \sum A_i(s_1) + \sum B_i(s_2) + \sum C_i(s_3) + \sum D_i(s_4) \tag{4}$$

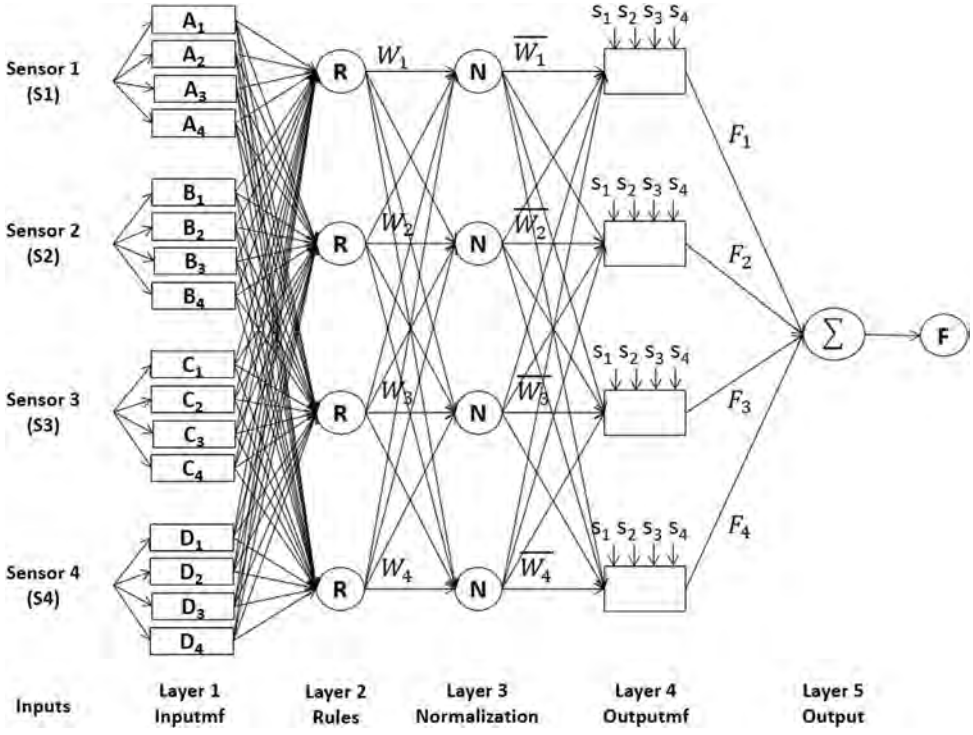


**Fig. 11.** ANFIS architecture model for the walking phase classification.

where R is the rule, and W is the weight of the rule. Each node is the firing strength of a rule.

The next is the normalization layer with non-adaptive nodes. Each node calculates the ratio of the rule's firing strength to the sum of all rules' firing strength. The outputs are called normalized firing strengths. The third layer guarantees stable convergence of weights, biases, and avoids the time-consuming process of defuzzification.

$$\overline{W} = \frac{W_i}{\sum W_i} = \frac{W_i}{W_1 + W_2 + W_3 + W_4} \tag{5}$$

The fourth layer is the defuzzification layer with all adaptive nodes, which used to de-fuzzify membership functions (MFs) to obtain the output.

$$W_i\bar{F}_i = W_i\bar{(}p_i s_1 + q_i s_2 + r_i s_3 + k_i s_4\,) \tag{6}$$

where $\overline{W}$ is the normalized firing strength from the previous layer (layer three output), and {p, q, r, k} is the corresponding consequent parameters set of this node.

The last layer (5th) is the summation layer. The single non-adaptive node in this layer is a fixed node, which computes the overall outputs as the summation of all incoming signals.

$$\sum W_i F_i\bar{=} \frac{\sum W_i\bar{F}_i}{\sum W_i\bar{}} = \frac{W_1\bar{F}_1 + W_2\bar{F}_2 + W_3\bar{F}_3 + W_4\bar{F}_4}{W_1\bar{+}W_2\bar{+}W_3\bar{+}W_4\bar{}} \tag{7}$$

This research proposes a hybrid learning algorithm in order to optimize the ANFIS values. The learning process of the neural network will change the values of membership functions (MFs), as well as minimize the error through the sum of the squared difference between the output and the real signal. Otherwise, we also design the fuzzy c-means algorithm (FCM) [48] in order to optimize the fuzzy sets and the fuzzy inference rules. FCM is a method of clustering that allows one piece of data to belong to more clusters. It is based on the minimization of the following objective function:

$$J_m = \sum_{i=1}^{D}\sum_{j=1}^{N}\mu_{ij}^{m}\left\|x_i - c_j\right\|^2 \tag{8}$$

where D represents the number of data points, N represents the number of clusters, $\mu_{ij}$ is the degree of membership of $x_i$ in the $j_{th}$ cluster, $m$ is real number greater than 1, $x_i$ is the $i_{th}$ data point, and cj is the center of the $j_{th}$ cluster.

The ANFIS model was developed on Matlab 2017b software. The specifications of this model are shown in Table 1:

**Table 1**
Parameters of ANFIS model.

| Parameter | Description |
|---|---|
| Type | 'sugeno' |
| Number of nodes | 64 |
| Number of training data pairs | 600 |
| Number of fresh data pairs | 200 |
| Number of fuzzy rules | 20 |

Specifically, the ANFIS model used the Sugeno-type fuzzy inference system and the FCM algorithm. Each cluster contains one fuzzy rule and one membership function for each input/output variable. So, there are 20 rules. The performance of this ANFIS model was demonstrated through the classification of different walking phases in a real application. A set of 1000 phase samples were recorded from the experimental. Eight hundred samples (80 %) were set up for constructing the model, and 200 samples (20 %) were utilized for evaluating the system.

Results of the experiment show the model output and the correct phase of gait. Fig. 12 shows the accuracy and confusion matrix of training and fresh data. The diagonal elements represent the number of cases for which the classified phase is equal to the actual phase, while off-diagonal elements are those that are mislabeled. The high diagonal values of the confusion matrix

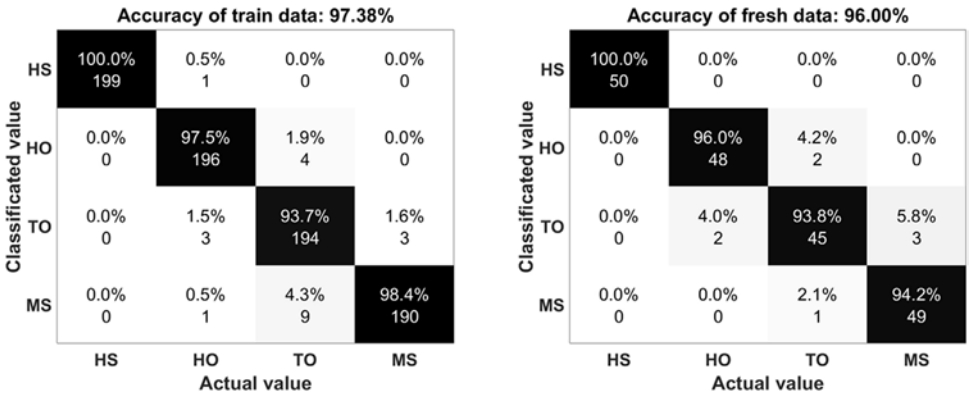


**Fig. 12.** Confusion matrix results of the walking phase classification.

demonstrate many correct classifications. Accordingly, the ANFIS algorithm obtained a mean performance accuracy of 97 % on training data and 96 % on fresh data. This accuracy indicates that there is a good agreement between the measured and classified values. The HS phases are easy to classify with high accuracy (~ 100 %), and respectively. Besides, the HO phases have a lower accuracy at 96 % and could be confused with TO phases (4 %). The MS phases have accuracy at 94 %, and the TO phases have the lowest accuracy at 93 %.

## 6. Conclusions

In summary, a capacitive pressure sensor-based-spacer fabric was presented with a highly sensitive/elastic, and very fast response time. For the electrode layers, a highly conductive fabric was obtained by printing SWCNT/silver inks in order to increase durability under large deformations. The dielectric was a network of the PET yarns and the encapsulation paste in order to guarantee robust recovery ability. For sensitive applications, we proposed the smart textile glove for grasping the objects. And finally, we developed a complete combination of the sensors on smart socks and the ANFIS module to analyze the phases of walking gait with high accuracy. These applications demonstrated the fabricated sensors could be used in a large range of wearable applications in robot control or human motion recognition field.

## Declaration of Competing Interest

None

## Acknowledgments

This research was supported by Korea Institute for Advancement of Technology (KIAT) grant funded by the Korea Government (MOTIE) (P0012770).

## Appendix A. Supplementary data

Supplementary material related to this article can be found, in the online version, at doi:https://doi.org/10.1016/j.sna.2020.112029.

## References

[1] S. Seyedin, P. Zhang, M. Naebe, S. Qin, J. Chen, X. Wanga, J.M. Raza, Textile strain sensors: a review of the fabrication technologies, performance evaluation and applications, Mater. Horiz. 6 (2019) 219–249.
[2] Y. Huang, X. Fan, S.-C. Chen, N. Zhao, Emerging technologies of flexible pressure sensors: materials, modeling, devices, and manufacturing, Adv. Funct. Mater. 29 (2019), 1808509.
[3] L.M. Castano, A.B. Flatau, Smart fabric sensors and e-textile technologies: a review, Smart Mater. Struct. 23 (2014) 053001–053028.
[4] M. Stoppa, A. Chiolerio, Wearable electronics and smart textiles: a critical review, Sensors 14 (2014) 11957–11992.
[5] O.Y. Kweon, S.J. Lee, J.H. Oh, Wearable high-performance pressure sensors based on three-dimensional electrospun conductive nanofibers, NPG Asia Mater. 10 (2018) 540–551.
[6] L. Natta, V.M. Mastronardi, F. Guido, L. Algieri, S. Puce, F. Pisano, F. Rizzi, R. Pulli, A. Qualtieri, M.D. Vittorio, Soft and flexible piezoelectric smart patch for vascular graft monitoring based on aluminum nitride thin film, Sci. Rep. 9 (2019) 8392–8402.
[7] X. Li, H. Hu, T. Hua, B. Xu, S. Jiang, Wearable strain sensing textile based on one-dimensional stretchable and weavable yarn sensors, Nano Res. 11 (2018) 5799–5811.
[8] Q. Li, H. Chen, Z.-Y. Ran, L.-N. Zhang, R.-F. Xiang, X. Wang, X.-M. Tao, X. Ding, Full fabric sensing network with large deformation for continuous detection of skin temperature, Smart Mater. Struct. 27 (2018) 105017–105029.
[9] P. Lugoda, T. Hughes-Riley, R. Morris, T. Dias, A wearable textile thermograph, Sensors 18 (2018) 2369–2391.
[10] W.V. Gonzales, A.T. Mobashsher, A. Abbosh, The progress of glucose monitoring—a review of invasive to minimally and non-invasive techniques, devices and sensors, Sensors 19 (2019) 800–845.
[11] Y. Zhang, Y. Chen, T. Man, D. Huang, X. Li, H. Zhu, Z. Li, High resolution non-invasive intraocular pressure monitoring by use of graphene woven fabrics on contact lens, Microsyst. Nanoeng. 5 (2019) 39–47.
[12] J. Kim, A.S. Campbell, B.E.-F. de Ávila, J. Wang, Wearable biosensors for healthcare monitoring, Nat. Biotechnol. 37 (2019) 389–406.
[13] Y. Zhou, J. He, H. Wang, K. Qi, N. Nan, X. You, W. Shao, L. Wang, B. Ding, S. Cui, Highly sensitive, self-powered and wearable electronic skin based on pressure-sensitive nanofiber woven fabric sensor, Sci. Rep. 7 (2017) 12949–12958.
[14] M. Bariya, H.Y.Y. Nyein, A. Javey, Wearable sweat sensors, Nat. Electron. 1 (2018) 160–171.
[15] H. Jin, N. Matsuhisa, S. Lee, M. Abbas, T. Yokota, T. Someya, Enhancing the performance of stretchable conductors for E-textiles by controlled ink permeation, Adv. Mater. 29 (2017) 1605848–1605856.
[16] S. Yao, P. Swetha, Y. Zhu, Nanomaterial-enabled wearable sensors for healthcare, Adv. Healthcare Mater. 7 (2018) 1700889–1700916.
[17] X. Liao, W. Song, X. Zhang, H. Huang, Y. Wang, Y. Zheng, Directly printed wearable electronic sensing textiles towards human–machine interfaces, J. Mater. Chem. C 6 (2018) 12841–12848.
[18] C.G. Núñez, L. Manjakkal, R. Dahiya, Energy autonomous electronic skin, NPJ Flexible Electron. 3 (2019) 1–24.
[19] M. Liu, X. Pu, C. Jiang, T. Liu, X. Huang, L. Chen, C. Du, J. Sun, W. Hu, Z.L. Wang, Large-area all-textile pressure sensors for monitoring human motion and physiological signals, Adv. Mater. 29 (2017) 1703700–1703709.
[20] Z. Wang, Y. Si, C. Zhao, D. Yu, W. Wang, G. Sun, Flexible and washable poly(Ionic liquid) nanofibrous membrane with moisture proof pressure sensing for real-life wearable electronics, ACS Appl. Mater. Interfaces 11 (2019) 27200–27209.
[21] R. Wu, L. Ma, C. Hou, Z. Meng, W. Guo, W. Yu, R. Yu, F. Hu, X.Y. Liu, Silk composite electronic textile sensor for high space precision 2D combo temperature–pressure sensing, Small 15 (2019) 1901558–1901569.
[22] T. Huang, S. Yang, P. He, J. Sun, S. Zhang, D. Li, Y. Meng, J. Zhou, H. Tang, J. Liang, G. Ding, X. Xie, Phase-separation-induced PVDF/Graphene coating on fabrics toward flexible piezoelectric sensors, ACS Appl. Mater. Interfaces 10 (2018) 30732–30740.
[23] M. Pruvost, W.J. Smit, C. Monteux, P. Poulin, A. Colin, Polymeric foams for flexible and highly sensitive low-pressure capacitive sensors, NPJ Flexible Electron. 3 (2019) 7–13.
[24] O. Atalay, A. Atalay, J. Gafford, C. Walsh, A highly sensitive capacitive-based Soft pressure sensor based on a conductive fabric and a microporous dielectric layer, Int. J. Adv. Mater. Technol. 3 (2018) 1700237–1700245.

[25] S. Wan, H. Bi, Y. Zhou, X. Xie, S. Su, K. Yin, L. Sun, Graphene oxide as high-performance dielectric materials for capacitive pressure sensors, Carbon 114 (2017) 209–216.
[26] R. Li, Y. Si, Z. Zhu, Y. Guo, Y. Zhang, N. Pan, G. Sun, T. Pan, Supercapacitive iontronic nanofabric sensing, Adv. Mater. 29 (2017) 1700253–1700261.
[27] J.S. Heo, J. Eom, Y.-H. Kim, S.K. Park, Recent progress of textile-based wearable electronics: a comprehensive review of materials, devices, and applications, Small 14 (2018) 1703034–1703050.
[28] L.-C. Jheng, C.-H. Hsiao, W.-C. Ko, S.L.-C. Hsu, Y.-L. Huang, Conductive films based on sandwich structures of carbon nanotubes/silver nanowires for stretchable interconnects, Nanotechnology 20 (2019) 23–53.
[29] S. Ding, J. Jiu, Y. Gao, Y. Tian, T. Araki, T. Sugahara, S. Nagao, M. Nogi, H. Koga, K. Suganuma, H. Uchida, One-step fabrication of stretchable copper nanowire conductors by a fast photonic sintering technique and its application in wearable devices, ACS appl. Mater. Interfaces 8 (2016) 6190–6199.
[30] DM-SIP-2001 - Dycotec Materials, 2019 (Accessed on 22 September 2019) https://www.dycotecmaterials.com/product/dm-sip-2001/.
[31] DM-ENC-2500 - Dycotec Materials, 2019 (Accessed on 22 September 2019) https://www.dycotecmaterials.com/product/dm-enc-2500/.
[32] S. Rajendran, Advanced Textiles for Wound Care, 2nd ed., Woodhead Publishing, Cambridge, United Kingdom, 2018.
[33] C.H. Lim, E. Vats, C.S. Chan, Fuzzy human motion analysis: a review, Pattern Recognit. 48 (2015) 1773–1796.
[34] A. Bulsari, H. Saxén, A. KrasŁawski, Fuzzy simulation by an artificial neural network, Eng. Appl. Artif. Intell. 5 (1992) 401–406.
[35] J. Han, C. Moraga, S. Sinne, Optimization of feedforward neural networks, Eng. Appl. Artif. Intell. 9 (1996) 109–119.
[36] S.-Y. Chiang, Y.-C. Kan, Y.-S. Chen, Y.-C. Tu, H.-C. Lin, Fuzzy computing model of activity recognition on WSN movement data for ubiquitous healthcare measurement, Sensors 16 (2016) 2053–2075.
[37] W. Caesarendra, T. Tjahjowidodo, Y. Nico, S. Wahyudati, L. Nurhasanah, EMG finger movement classification based on ANFIS, J. Phys. Conf. Ser. 1007 (2018) 012005–012012.
[38] C. Mummolo, L. Mangialardi, J.H. Kim, Quantifying dynamic characteristics of human walking for comprehensive gait cycle, J. Biomech. Eng. 135 (2013) 091006–091016.
[39] A. Muro-de-la-Herran, B. Garcia-Zapirain, A. Mendez-Zorrilla, Gait analysis methods: an overview of wearable and non-wearable systems, highlighting clinical applications, Sensors 14 (2014) 3362–3394.
[40] X. Lü, X. Li, F. Zhang, S. Wang, D. Xue, L. Qi, H. Wang, X. Li, W. Bao, R. Chen, A novel proximity sensor based on parallel plate capacitance, IEEE Sens. J. 18 (2018) 7015–7022.
[41] H. Jin, S. Jung, J. Kim, S. Heo, J. Lim, W. Park, H.Y. Chu, F. Bien, K. Park, Stretchable dual-capacitor multi-sensor for touch-curvature-pressure-strain sensing, Sci. Rep. 7 (2017) 10854–10862.
[42] R. Wu, L. Ma, A. Patil, C. Hou, S. Zhu, X. Fan, H. Lin, W. Yu, W. Guo, X.Y. Liu, All-textile electronic skin enabled by highly elastic spacer fabric and conductive fibers, ACS Appl. Mater. Interfaces 11 (2019) 33336–33346.
[43] Y. Zhang, Z. Lin, X. Huang, X. You, J. Ye, H. Wu, Highly sensitive capacitive pressure sensor with elastic metallized sponge, Smart Mater. Struct. 28 (2019) 105023.
[44] Z. He, W. Chen, B. Liang, C. Liu, L. Yang, D. Lu, Z. Mo, H. Zhu, Z. Tang, X. Gui, Capacitive pressure sensor with high sensitivity and fast response to dynamic interaction based on graphene and porous nylon networks, ACS Appl. Mater. Interfaces 10 (2018) 12816–12823.
[45] A. Atalay, V. Sanchez, O. Atalay, D.M. Vogt, F. Haufe, R.J. Wood, C.J. Walsh, Batch fabrication of customizable silicone-textile composite capacitive strain sensors for human motion tracking, Int. J. Adv. Mater. Technol. 2 (2017) 1700136–1700144.
[46] Teensy USB Development Board, 2019 (Accessed on 22 September 2019) https://www.pjrc.com/store/teensy32.html.
[47] C. Vu, J. Kim, Human motion recognition using e-textile sensor and adaptive neuro-fuzzy inference system, Fibers Polym. 19 (2018) 2657–2666.
[48] S. Miyamoto, H. Ichihashi, K. Honda, BasicMethods for c-means clustering, in: S. Miyamoto, H. Ichihashi, K. Honda (Eds.), Algorithms for Fuzzy Clustering, Springer, Berlin, 2008, pp. 9–42.

## Biographies

**Chi Cuong Vu** received his B.S. in Electronic & Telecommunication in 2014, Vietnam. He finished M.S. program in Organic materials and fiber engineering at Soongsil University, Seoul, Korea. He is currently a Ph.D. student in Organic Materials and Fiber Engineering at R&D Center, Soongsil University, Seoul, Korea. His research interests include flexible-stretchable electronic materials and their application in wearable human-activity monitoring and personal healthcare.

**Jooyong Kim** received the B.S. and M.S. degree in fiber and polymer science & engineering from Seoul National University, Seoul, Korea, in 1990 and 1992, respectively. He is currently working as a professor at department of organic materials and fiber engineering of Soongsil University, Seoul, Korea since 1999 after Ph.D. at North Carolina State University, Raleigh, USA. From 1998 to 1999, he was a post-doctoral researcher at department of mechanical & aerospace engineering of UCLA, California, USA. His research interest includes the development of smart fashion products based on electronic textiles.